A Linearized Path Integral Description of the Collision Process between a Water Molecule and a Graphite Surface

Nikola Marković*

Physical Chemistry, Department of Chemical and Biological Engineering, Chalmers University of Technology, SE-412 96 Göteborg, Sweden

Jens A. Poulsen

Physical Chemistry, Department of Chemistry, Göteborg University, SE-412 96 Göteborg, Sweden

Received: June 22, 2007; In Final Form: December 5, 2007

Quantum effects in the scattering and desorption process of a water molecule from a graphite surface are investigated using the linearized path integral model. The graphite surface is quantized rigorously using the fully quantum many-body Wigner transform of the surface Boltzmann operator, while the water molecule is treated as rigid. Classical dynamics with these quantized initial conditions show that quantizing the surface at 100 and 300 K results in markedly different results, compared to a fully classical analysis. The trapping probability (defined as the probability of multiple encounters with the surface) is not sensitive to the choice of dynamical treatment, but the residence time on the surface is much shorter in the quantum case. At 300 K the transiently trapped molecules desorb from the surface with a rate constant which is 60−70% larger than the corresponding classical value. Lowering the surface temperature to 100 K decreases the quantum rate constant by approximately a factor of 3 while all trapped molecules stick to the surface in the classical case. The stability of the quantum initial state for the highly anisotropic graphite crystal is discussed in detail as well as the dynamical consequences of energy redistribution during the scattering process. The graphite surface application demonstrates that the Boltzmann operator Wigner transform for a system with 900 degrees of freedom can be obtained by the so-called gradient implementation [Poulsen et al. *J. Chem. Theory Comput.* **2006**, 2, 1482] of the underlying Feynman−Kleinert effective frequency theory, an implementation that only requires a force and potential routine for the system at hand, and hence is applicable to any molecule−surface collision problem.

1. Introduction

Many important chemical processes in the environment and in industrial applications occur at surfaces. Examples include reactions on ice particles in the atmosphere and the interstellar medium, heterogeneous catalysis, epitaxial growth and corrosion. Theoretical studies of the dynamics of such processes are very important in order to obtain a detailed understanding of the chemistry and physics involved. Dissociative adsorption of molecules on surfaces is a key step in heterogeneous catalysis. The dissociative adsorption of H_2 on metals can be considered as a prototype reaction and has been studied extensively. Over the past decade advances in computer technology and, in particular, the development of efficient computational techniques have made quantum dynamical studies of hydrogen scattering from metal surfaces possible.[1−11] These impressive calculations, which include all six molecular H_2 degrees of freedom, have provided detailed information regarding sticking and dissociation probabilities and how these quantities depend on the magnitude and direction of the incident velocity and the vibrational and rotational excitation of the impinging H_2 molecule. The studies mentioned above all assume a rigid surface, i.e., there is no energy transfer to the substrate. This approximation is motivated by the large mass difference between the hydrogen molecule and the metal atoms.[3,8] Although not dominant, thermal effects have been observed experimentally[12] and have also been accounted for approximately in quantum dynamical studies.[13]

To rigorously include the effect of the phonons and allow for energy dissipation in a quantum dynamical study of a realistic surface scattering problem is a very demanding task usually requiring approximations.[14] In one approach the density matrix is propagated using the Liouville−von Neumann equation.[15] Usually one considers open systems (and the reduced density matrix) where the Liouvillian is written as a sum of a Hamiltonian and a dissipative part. The dissipative part may be described using the so-called dynamical semi-group formalism[16−20] or using a perturbative approach ("Redfield theory'').[21−25] A coupled wave vector description of the density matrix has been developed relaxing the requirements of weak coupling and rapid bath relaxation.[26,27] Surface scattering problems have also been treated using quantum mechanical mean field methods,[28,29] classical[30] and semi-classical[31] generalized Langevin schemes or other mixed quantum−classical approaches.[32−34] Estimates of trapping and sticking probabilities can also be obtained using nondissipative low-dimensional quantum[35] or classical models.[36]

Our previous surface scattering work has been focused on scattering of atoms,[37] polyatomic molecules[38,39] and large clusters[40−42] from graphite surfaces. The simulations were carried out in cooperation with experimentalists in order to interpret results from molecular beam studies. In these calculations we used a stochastic trajectory method. All surface atoms

* Corresponding author. E-mail: nikola@chalmers.se.

10.1021/jp074875c CCC: $40.75
Published on Web 02/02/2008

were treated classically. The first (bottom) layer of the graphite crystal was held fixed. For atoms in the second layer the equations of motion were modified by adding stochastic and friction forces related to the Debye temperatures ($\theta_{D,x} = \theta_{D,y} = 2400$ K, $\theta_{D,z} = 1200$ K) relevant for our graphite potential.[37,38] The model has performed well, and we have been able to simulate experimental results over a wide range of initial conditions. The choice of a classical description was rather natural for these studies where many different sets of initial conditions had to be considered and a large crystal was required since the collision energy was quite high in some cases. In addition, it turned out that multiple collisions were important leading to long propagation times.

The scattering studies mentioned above have been carried out at surface temperatures in the range $T_s = 300-1400$ K, but most of the calculations have been for rather hot surfaces. For low surface temperatures quantum effects may be significant due to the high Debye temperatures for graphite. The purpose of the present work is to investigate the importance of quantum effects when the graphite surface is at low or intermediate temperatures. For this purpose the classical Wigner (CW) model[43−48] is used.

The CW model is conceptually very simple. It utilizes Wigner's celebrated phase-space formulation of quantum mechanics.[49] Quantum dynamical problems are dealt with by CW in a manner that strongly resembles that of ordinary classical mechanics. A CW calculation can be divided into a two-step procedure: (i) sample position and momenta, (q,p)'s, from the quantum phase-space Wigner transform of the relevant system density operator; (ii) then, using the (q,p)'s, perform classical dynamics and compute the relevant dynamical quantities. Hence, CW differs from a pure classical treatment only by the initial conditions. In the present problem, the appropriate quantum initial conditions for the surface atoms are sampled from Wigner's phase-space distribution of the graphite surface Boltzmann operator.

The CW method can be derived from a linearization of a Feynman path integral representation[43] of the quantity of interest. Hence, the method is therefore also referred to as the linearized path integral (LPI) approximation. In the following, the two acronyms CW and LPI will be used interchangeably, as they are formally equivalent.

The classical dynamical treatment is obviously a great simplification, leading to the exclusion of dynamical quantum effects. The implication of this is the well-known fact that LPI is only accurate for short times (see, e.g., ref 50 for a classic example). It is, however, exact for harmonic systems and in the high-temperature limit. An efficient method to generate the initial conditions (given by the Boltzmann operator) is still required if the scheme should be practical. In ref 43 Poulsen and co-workers demonstrated that an approximate but still quite accurate Boltzmann operator Wigner transform could be obtained, by applying the effective frequency variational theory due to Feynman and Kleinert (FK). The resulting method, which combines the FK Boltzmann Wigner transform with LPI dynamics, is referred to as FK-LPI.

The FK-LPI methodology has recently been applied for computing velocity correlation functions (CF)'s and Van Hove CFs for a number of nontrivial condensed phase problems (see ref 47 and references therein). The results have been very encouraging and show that the FK-LPI method is able to compute the early time-dynamics of the CF's with a reasonable accuracy. One should note that, in condensed phase, the CF's decay to zero typically after a few picoseconds and hence the LPI method is then only required to be a reasonable short time theory.

In this paper we apply FK-LPI to collision processes where molecules are trapped on a surface for up to several tens of picoseconds. The application of a short-time theory to this type of problem is obviously problematic. In particular the residence time of transiently trapped molecules is sensitive to the precise energy distribution of the surface atoms, but as we shall see, a desorption-like rate constant may still be extracted from the short-time behavior of the trapping probability.

The FK-LPI method is in the present paper implemented in two ways, which differ in the way the surface Wigner transform is calculated. First, we adopt the general so-called gradient sampling implementation[47] which only requires a standard force routine to work. The results of this method are compared to a more approximate, but faster method, and we show that the latter is indeed accurate enough for the present application. The system considered in the present work is a reasonably realistic model of a rigid water molecule scattering from a graphite surface[39] previously treated classically in connection with an experimental study.

The LPI and Feynman−Kleinert effective frequency theory are presented in section 2. In section 3 we then proceed and consider the graphite model, the sampling of the initial phase-space conditions and the dynamical calculations. Our results are presented and discussed in section 4. The main conclusions are finally summarized in Section 5.

2. Theory

The basic idea behind the classical Wigner (CW) approximation to quantum dynamics was essentially first presented by Heller.[51] He suggested the idea of propagating nonstationary Wigner phase-space distributions by running a swarm of classical trajectories. More recently,[43,52,53] the same idea has been used to formulate the calculation of correlation functions (CF's), $\langle \hat{A}(0)\hat{B}(t)\rangle$, where the CW approximation reads

$$\langle \hat{A}(0)\hat{B}(t)\rangle \approx \frac{1}{(2\pi\hbar)^{3N}}\int\int \frac{dq\, dp}{Z}(\exp(-\beta\hat{H})\hat{A})_W[q,p](\hat{B})_W[q_t,p_t] \quad (1)$$

which follows directly from the exact path integral (PI) expression by carrying out the linearization procedure.[43] Equation 1 may be interpreted/implemented as follows: Phase-space points (q,p) are sampled from the Wigner transform of $\exp(-\beta\hat{H})\hat{A}$, the transform $(\hat{C})_W[x,p]$ being defined for an arbitrary operator $\hat{C}$ by

$$(\hat{C})_W[x,p] \equiv \int_{-\infty}^{+\infty} d\eta\, \exp(-ip\eta/\hbar)\left\langle x+\frac{1}{2}\eta\middle|\hat{C}\middle|x-\frac{1}{2}\eta\right\rangle \quad (2)$$

In eq 1 (q,p) are evolved classically according to the Hamiltonian $H(q,p)$ to (q_t,p_t) which serve as the phase-space arguments of $(\hat{B})_W[q_t,p_t]$. $3N$ is the dimensionality of the problem.

In the present study, we will not be interested in CF's, but instead, for instance, we want to know the fraction of water molecules that stay on the surface after a time t. The quantity of interest still follows from eq 1, if we make the substitutions

$$\hat{A} \rightarrow 1, \quad \exp(-\beta\hat{H}) \rightarrow \exp(-\beta\hat{H}_C) \times \hat{\rho}_{H_2O}$$

and

$$(\hat{B})_W[q_t,p_t] = \begin{cases} 1 & q_t \text{ is on surface} \\ 0 & \text{otherwise} \end{cases} \quad (3)$$

where $\hat{H}_C$ and $\hat{\rho}_{H_2O}$ are the graphite Hamiltonian and free water molecule density operator, respectively.

2.1. Feynman−Kleinert Approximation to the Wigner Transform. A practical route to the Wigner transform of the operator $\exp(-\beta\hat{H})\hat{A}$ for complex systems is required to implement LPI.[43] The approach we use is based on combining the effective frequency variational theory of Feynman and Kleinert (FK)[54] with the quasi-density operator formalism of Jang and Voth.[55] The approach exploits the classical centroid phase-space variables (x_c,p_c), where

$$x_c = \frac{1}{\beta\hbar}\int_0^{\beta\hbar} d\tau\, x(\tau) \quad (4)$$

and p_c is a similarly defined centroid momentum. Presented in formal terms, in one dimension, one may approximate the Boltzmann operator by[43]

$$\exp(-\beta\hat{H}) \approx \int\int dx_c\, dp_c\, \rho_{FK}(x_c,p_c)\, \hat{\delta}_{FK}(x_c,p_c) \quad (5)$$

where $\rho_{FK}(x_c,p_c)$ is the FK approximation to the centroid phase-space density,

$$\rho_{FK}(x_c,p_c) = \frac{1}{2\pi\hbar}\exp\left(-\beta\frac{p_c^2}{2M}\right)\exp(-\beta W_1(x_c)) \quad (6)$$

and $W_1(x_c)$ is the corresponding FK approximation to the centroid potential. Equation 5 is very practical, since the operators $\hat{\delta}_{FK}(x_c,p_c)$ have a simple Wigner transform, see below. The Wigner transform of $\exp(-\beta\hat{H})$ may then be obtained by sampling Wigner transforms of operators $\hat{\delta}_{FK}(x_c,p_c)$. Hence the computational scheme involves a Monte Carlo walk in the variables (x_c,p_c) with weight function $\rho_{FK}(x_c,p_c)$, thereby generating a sequence of $\hat{\delta}_{FK}$ operators. The operator $\hat{\delta}_{FK}(x_c,p_c)$ is the so-called effective frequency quasi-density operator (QDO):

$$\hat{\delta}_{FK}(x_c,p_c) = \int\int dx\, dx' \sqrt{\frac{M\Omega(x_c)}{\pi\hbar\alpha}}|x'\rangle\langle x| \times \exp\left\{ i\frac{p_c}{\hbar}(x'-x) - \frac{M\Omega(x_c)}{\hbar\alpha}\left(\frac{x+x'}{2}-x_c\right)^2 - \frac{M\Omega(x_c)\alpha}{4\hbar}(x'-x)^2\right\} \quad (7)$$

where α is a function of the *effective* frequency, $\Omega(x_c)$, through the relation

$$\alpha = \coth\left(\frac{\Omega(x_c)\hbar\beta}{2}\right) - \frac{2}{\Omega(x_c)\hbar\beta} \quad (8)$$

and the quantity α is related to the *smearing width* $a^2(x_c)$[54] through

$$a^2(x_c) = \hbar\alpha/2M\Omega(x_c) \quad (9)$$

This width measures the thermal quantum "smearing'' around the classical-like position x_c. To close the equations, the effective frequency is given by the mass-weighted classical Hessian averaged over the length $a^2(x_c)$:

$$\Omega^2(x_c) = \frac{1}{M}\int dy \frac{1}{\sqrt{2\pi a^2(x_c)}} V''(x_c+y)\exp\left(-\frac{1}{2}y^2/a^2(x_c)\right) \quad (10)$$

This FK prescription gives the best local harmonic description of the potential surface, based on a system free energy criterion.[54] To obtain $\Omega^2(x_c)$ and $a^2(x_c)$, eqs 8−10 are solved iteratively.[47] $W_1(x_c)$ can then be calculated once $\Omega^2(x_c)$ and $a^2(x_c)$ are converged,[47] and the only remaining effort is an evaluation of the smeared potential, $V_{a^2}(x_c)$,

$$V_{a^2}(x_c) = \int dy \frac{1}{\sqrt{2\pi a^2(x_c)}} V(x_c+y)\exp\left(-\frac{1}{2}y^2/a^2(x_c)\right) \quad (11)$$

which is needed in the expression for the centroid potential:[43]

$$W_1(x_c) = k_B T \ln\left(\frac{\sinh\left(\frac{\hbar\Omega(x_c)}{2k_BT}\right)}{\frac{\hbar\Omega(x_c)}{2k_BT}}\right) + V_{a^2}(x_c) - \frac{1}{2}Ma^2(x_c)\,\Omega^2(x_c) \quad (12)$$

Wigner-transforming eq 5 then amounts to transforming $\hat{\delta}_{FK}$, eq 7, which can be done analytically:

$$(\hat{\delta}_{FK}(x_c,p_c))_W[q,p] = \frac{2}{\alpha}\exp\left(-\frac{M\Omega(x_c)}{\hbar\alpha}(q-x_c)^2 - \frac{1}{M\Omega(x_c)\alpha\hbar}(p-p_c)^2\right) \quad (13)$$

As is evident from eqs 5−7, the variable p_c may be integrated out analytically from these equations. This leads to the following overall Wigner transform of the Boltzmann operator:

$$(\exp(-\beta\hat{H}))[q,p] \approx \int\frac{dx_c}{2\pi\hbar}\exp(-\beta W_1(x_c))\sqrt{\frac{M\alpha\pi}{\frac{\beta}{2}\coth(\hbar\Omega(x_c)\beta/2)}} \times \frac{2}{\alpha}\exp\left(-\frac{M\Omega(x_c)}{\hbar\alpha}(q-x_c)^2 - \frac{\tanh(\hbar\Omega(x_c)\beta/2)}{M\Omega(x_c)\hbar}p^2\right) \quad (14)$$

Equation 14 constitutes our basic Wigner transform implementation to be used in this work. For the multidimensional version of these equations, we refer to ref 47.

2.2. Gradient Sampling: The General Boltzmann Operator Wigner Transform Implementation. For a realistic model of a graphite surface, we cannot expect the potential function to be simple (e.g., pairwise). Equations 10 and 11 must then be evaluated numerically. We have recently put forth a method for doing this.[47]

This procedure only requires a routine that provides the potential and its gradient. These are available in any molecular dynamics code. To derive this method, we first consider eq 10 in the multidimensional case:

$$\underline{\Omega}^2(\vec{z}_c) = \int d\vec{z}\, \frac{1}{\sqrt{||2\pi\underline{A}(\vec{z}_c)||}}\underline{M}^{-1/2}\underline{H}(\vec{z})\underline{M}^{-1/2} \times \exp\left(-\frac{1}{2}(\vec{z}-\vec{z}_c)^T A(\vec{z}_c)^{-1}(\vec{z}-\vec{z}_c)\right) \quad (15)$$

where $\underline{H}(\vec{z})$ is the Hessian matrix. We start by integrating eq 15 by parts, which leads immediately to

$$\underline{\Omega}^2(\vec{z}_c) = \int d\vec{z}\, \frac{1}{\sqrt{||2\pi\underline{A}(\vec{z}_c)||}}\, \underline{M}^{-1/2}\underline{\Delta}(\vec{z},\vec{z}_c)\underline{M}^{-1/2} \times \exp\left(-\frac{1}{2}(\vec{z}-\vec{z}_c)^T A(\vec{z}_c)^{-1}(\vec{z}-\vec{z}_c)\right) \quad (16)$$

where

$$\underline{\Delta}_{ij}(\vec{z},\vec{z}_c) = \{\sum_{k=1}^{3N}\{\underline{A}^{-1}\}_{kj}(z_k - z_{c,k})\} \times \frac{\partial}{\partial z_i} V(\vec{z}) \quad (17)$$

Hence, the scheme for calculating the smeared Hessian requires sampling vectors $\vec{z}$ around $\vec{z}_c$, and averaging to obtain the $(3N)^2$ quantities

$$\Gamma_{ij} = \left\langle (z_i - z_{c,i})\frac{\partial}{\partial z_j} V(\vec{z})\right\rangle \quad (18)$$

The (i,j)'th element of the smeared Hessian is then given by

$$\underline{\Omega}_{i,j}{}^2(\vec{z}_c) = m_i^{-1/2} m_j^{-1/2} \sum_{k=1}^{3N}\{\underline{A}^{-1}\}_{kj}\Gamma_{ki} \quad (19)$$

In practice, due to statistical errors in any finite sampling sequence, $\underline{\Omega}_{i,j}{}^2(\vec{z}_c)$ will not be symmetric, and this can be enforced by a "symmetrization'' procedure:

$$\underline{\Omega}_{i,j}{}^2(\vec{z}_c) \rightarrow (\underline{\Omega}_{i,j}{}^2(\vec{z}_c) + \underline{\Omega}_{j,i}{}^2(\vec{z}_c))/2 \quad (20)$$

Equation 11 is evaluated by direct sampling of vectors $\vec{z}$ around $\vec{z}_c$ as determined by the Gaussian weight function

$$\frac{1}{\sqrt{||2\pi\underline{A}(\vec{z}_c)||}} \exp\left(-\frac{1}{2}(\vec{z}-\vec{z}_c)^T\underline{A}(\vec{z}_c)^{-1}(\vec{z}-\vec{z}_c)\right) \quad (21)$$

3. The Water−Graphite System and Details of the Simulation

3.1. Water−Graphite System. Both the graphite and water−graphite potentials are taken from our previous study of water scattering from graphite.[39] The interaction within the graphene layers was described using Brenner's empirical potential,[56] and the interplanar forces were modeled using Morse functions.[38] A detailed discussion of the properties of the graphite model is given in ref 37. Three graphene layers with 150 carbon atoms in each were used to model the graphite crystal. In ref 39 five layers was used, but after repeating some of the calculations it was found that three layers was sufficient for the collision energies considered in the present study. Another difference is that stochastic and friction forces were not included in the present study. A detailed comparison of results from classical calculations with and without stochastic and friction forces showed only insignificant deviations. These tests were carried out for a surface temperature of 300 K, an incident angle of 30° and collision energies in the range 0.02 to 0.20 eV, i.e., the same initial conditions considered in the present study. By not including stochastic and friction forces the classical results can be compared directly to the results obtained using the FK-LPI method.

The water−graphite potential used in the present study is the potential denoted "Potential 1" in ref 39. The potential consists of Lennard-Jones contributions (O−C and H−C) and electrostatic contributions between point charges in H_2O and point quadrupoles centered on the carbon atoms. The potential is smoothly switched off as the water−carbon separation approaches 10 Å. The water molecule is treated as rigid with geometry and charge distribution taken from the RWK2 model.[57] The classical binding energy to a zero Kelvin graphite surface is 125 meV using this model.

3.2. Construction of Graphite FK Wigner Transform. We have in sections 2.1 and 2.2 described how to calculate the centroid potential defined for the multidimensional position $\vec{z}_c$. As already described, $\vec{z}_c$ is sampled from the classical-like centroid density, $\exp(-\beta W_1(\vec{z}_c))$, by Metropolis Monte Carlo,[58] and one thus needs a way of generating trial configurations. We adopt a trial step scheme formulated in terms of the classical graphite normal modes evaluated at the classical equilibrium geometry. Then, trial displacements are obtained as

$$\delta\eta_i = \eta_i^{\text{new}} - \eta_i^{\text{old}} = s(2\xi - 1)/\Omega_i, \quad i = 1, 3N \quad (22)$$

where η_i is the ith classical normal mode, ξ is a random number between zero and one, Ω_i is the frequency of normal mode i, and s is an overall scaling factor which is adjusted to ensure a reasonable overall acceptance ratio of the generated trial steps. Once a new trial normal mode vector is computed, the corresponding change in centroid geometry, $\delta\vec{z}_c$, is determined by a standard linear transformation, $\delta\vec{z}_c = \underline{U}\delta\vec{\eta}$, where $\underline{U}$ is fixed and defined via the classical normal modes at the equilibrium geometry of the graphite surface.

The number of iterations of the FK equations was 5 and 4 for $T = 100$ K and $T = 300$ K, respectively. To converge the smeared Hessian and potential, given by eqs 10 and 11, respectively, 30000 vectors $\vec{z}$ were sampled around $\vec{z}_c$ in both equations. The averaging over these vectors was distributed over 16 processors using a parallel implementation of the gradient sampling routine.

At $T = 300$ K, the surface was considered to be equilibrated after approximately 6600 centroid MC steps, see Figure 1. Then, a further 6000 centroid MC steps were performed and, for each 30th centroid position, ten phase-space points were sampled from eq 14 as initial conditions for classical dynamics. In the $T = 100$ K case, equilibration was achieved after some 9000 MC steps and afterward 3600 steps were performed and, again, for each 30th centroid position, ten phase-space points were sampled.

The rather small number of MC steps are sufficient since the colliding water molecule hits the surface at random positions. Hence, locally, the graphite surface atoms need not explore all possible phase-space configurations. Also, the lower temperature one considers, the less does the classical-like centroid coordinate $\vec{z}_c$ move, and eventually, at $T = 0$ K, only one centroid coordinate contributes to eq 14.

3.3. An Approximate FK Sampling. A more approximate but significantly faster implementation of the FK Wigner transform theory is to (i) replace the smeared Hessian, eq 10, by its classical counterpart, and (ii) replace the centroid potential in eq 12 by the classical potential. Then only a subroutine providing the surface Hessian is required and iterations are no longer necessary. From eq 10, it is obvious that approximation (i) is valid if the smearing width matrix is small. For an atom in the top layer, its 3×3 dimensional "self-part'' of the total $3N \times 3N$ dimensional smearing width matrix $\underline{A}(\vec{z}_c)$ is found to be approximately diagonal, with entries of size $a_{xx}{}^2 = 0.005$ bohr^2, $a_{yy}{}^2 = 0.005$ bohr^2 and $a_{zz}{}^2 = 0.009$ bohr^2. These smearing values are quite small: in fact they are more than an order of magnitude smaller than the values found in typical liquid applications,[47] which may be ascribed to the rather high

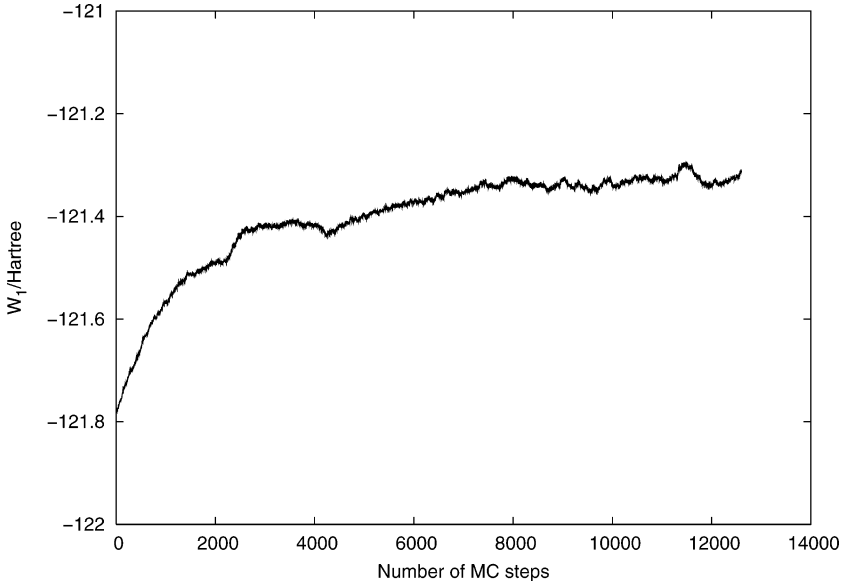

Figure 1. Equilibration of 300 K graphite surface. Centroid energy, W_1, of total graphite surface as a function of number of Monte Carlo steps.

surface frequencies which make $a^2(x_c)$ small, see eq 9. One should therefore expect that approximation (i) is well justified in the graphite case. Approximation (ii) is valid for high temperatures and for harmonic systems. In the latter case, the centroid potential and classical potential are identical except for an immaterial additive constant. In the following we will denote the simpler method, based on simplifications (i) and (ii), by approximate FK-LPI (AFK-LPI).

The AFK-LPI method is implemented by running classical dynamics for the surface and, for a given sampling interval, one calculates the instantaneous Hessian of the surface and construct the local QDO Wigner transform.

3.4. Dynamical Calculations. Molecular dynamics calculations have been carried out for rigid water molecules scattering off a graphite (0001) surface with a temperature of 100 or 300 K. Periodic boundary conditions were imposed in the x and y directions (the surface plane). The molecule was initially located outside the range of the gas-surface potential with its orientation and (x,y) position chosen at random. The parallel and perpendicular velocity components were chosen such that the molecule would hit the surface with an angle of 30° with respect to the surface normal and with the parallel velocity component in the $(11\bar{2}0)$ direction. Fixed translational energies in the range 0.02−0.20 eV were considered. The rotational energy of the molecule was sampled from a Boltzmann distribution at 200 K. The initial conditions for the surface atoms were in the classical case sampled from an equilibrated graphite crystal. In the FK-LPI/AFK-LPI cases the initial carbon positions and momenta were read from a file generated as described in sections 3.2−3.3. The equations of motion for the surface atoms were integrated using the velocity Verlet method, and the twelve equations of motion for the molecular degrees of freedom were solved using the Gear fourth order predictor-corrector scheme. The time step used was $\Delta t = 0.50$ fs. The trajectory was propagated until the water molecule was again outside the range of the potential or until the maximum time-limit (100 ps) was reached. For more details on the molecular dynamics calculations the reader is referred to ref 39.

4. Results and Discussion

Before discussing the scattering results, the properties of the FK-sampled graphite crystal will be considered. In Figure 2 the distribution of normal-mode frequencies obtained using the FK and AFK methods are compared. The AFK results at 100 and 300 K are based on 1000 and 4000 centroids, respectively. The accurate FK frequency distributions, obtained from single centroids, show considerably less structure due to the smearing of the potential in this case. Averaging over several centroids would make the FK distributions even smoother. Imaginary frequencies (shown as negative in the figure) appear for both the FK and AFK methods at 300 K, but the contribution from imaginary frequencies is much larger in the accurate FK case. At 100 K the AFK method yields only real frequencies. Overall

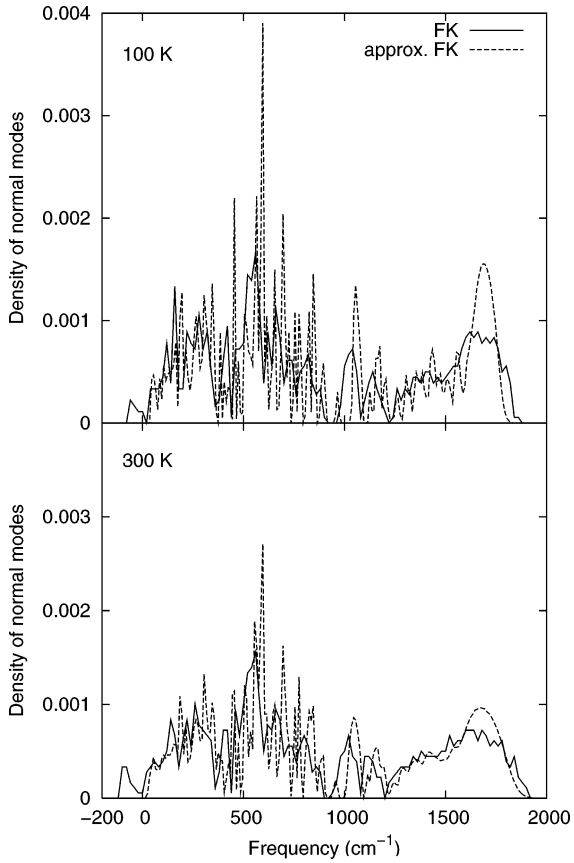

Figure 2. Frequency distribution for the graphite crystal at 100 and 300 K. Solid line, accurate FK; dashed line, approximate FK.

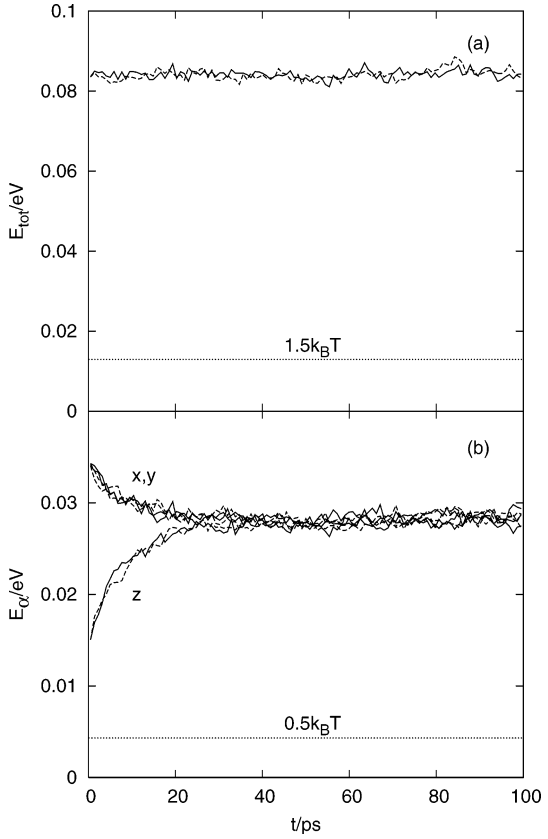

Figure 3. The time-dependence of the total kinetic energy (a) and the *x*-, *y*- and *z*-components (b) for atoms in the top layer. Solid lines, accurate FK-LPI; dashed lines, approximate FK-LPI. $T_s = 100$ K. Average over 10 trajectories.

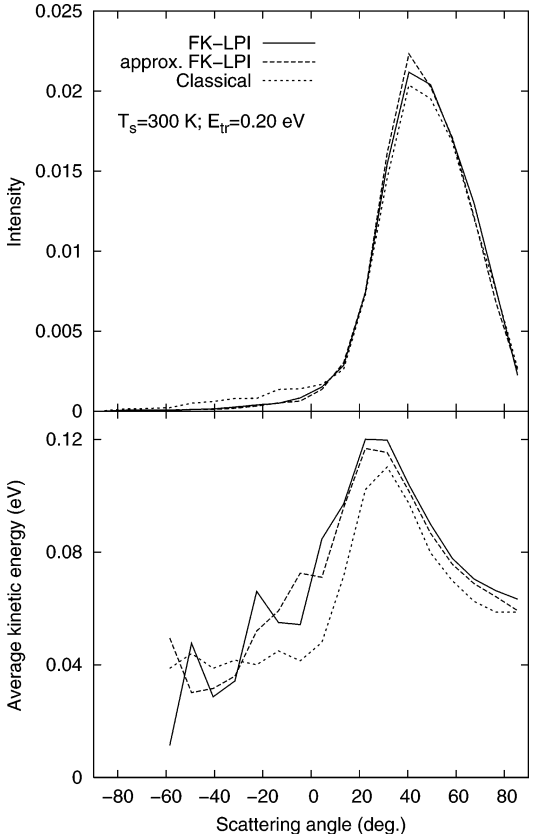

Figure 4. Angular distributions for H_2O scattering from graphite and average final kinetic energy as a function of the scattering angle. Initial conditions: $T_s = 300$ K, $E_{tr} = 0.20$ eV. Solid lines, accurate FK-LPI; dashed lines, approximate FK-LPI; dotted lines, classical.

the contribution to the spectra from imaginary frequencies is small compared to what has been observed previously for fluids.[43]

A general concern when using the classical Wigner method is the stability of the sampled quantum initial state ("conservation of ensemble''). In the present case the kinetic energy of the atoms in the top layer is of particular interest since they interact directly with the scattering molecule. In Figure 3 results are shown from a thermalized graphite surface ($T_s = 100$ K) propagated during 100 ps. No water molecule collides with the surface, i.e., the effects observed are only due to internal energy redistribution in the crystal. The large zero-point energy for graphite results in an average kinetic energy of 84 meV per atom compared to the classical value of 13 meV. This value is constant during the simulation which indicates that the kinetic energy is in equilibrium with the potential energy. The motion in the plane (*x*,*y*) is, however, not in equilibrium with the motion perpendicular (*z*) to the graphene layers. A considerable transfer of energy between parallel and the perpendicular motion occurs during the first 25 ps of the simulation. The deterioration of the initial quantum distribution will affect long-lived molecule−surface interactions. The growing kinetic energy in the perpendicular direction (from 15 to 28 meV) will increase the difference between the classical and quantum dynamics, in particular for long-lasting interactions. The difference between the classical and quantum kinetic energies in the *z*-direction is, however, large already at $t = 0$ (4.3 and 15 meV, respectively), implying that the effect of the changing energy distribution is quantitative and not qualitative. No difference is observed between the accurate and approximate FK sampling schemes.

Figure 4 shows results for H_2O molecules at 0.20 eV scattering from a graphite surface at 300 K. The angular distributions are very similar. The classical distribution is somewhat broader, and the corresponding final kinetic energy is lower. The differences between classical and quantum results become much more pronounced at lower translational energy, as shown in Figure 5 corresponding to 0.02 eV. Going from 0.20 to 0.02 eV increases the trapping probability (i.e., the probability of a molecule to experience multiple collisions with the surface) from about 0.54 to 0.85 irrespective of the dynamical treatment. The average residence time on the surface is, however, almost 2.5 times as long in the classical case compared to the quantum case, which explains the broader angular distribution. The results at a surface temperature of 100 K are very different, as is shown in Figure 6 for a collision energy of 0.20 eV. In this case the classical sticking probability is 0.54, i.e., 54% of the classically sampled trajectories are trapped at the surface for at least 100 ps. Of the remaining trajectories 85% correspond to direct scattering, i.e., they have only experienced a single collision with the surface, which explains the narrow angular distribution. An alternative comparison between classical and quantum angular distributions is shown in Figure 7 where the classical distribution now is a superposition of the inelastic distribution from Figure 6 with weight 0.46 and an equilibrium cosine law distribution with weight 0.54. In this way all trajectories are accounted for but with the assumption of complete thermalization of trajectories that are trapped for more than 100 ps. This type of two-component angular distribution has been observed experimentally for other systems.[59]

The expected effect on the angular distribution from an increased motion of the surface atoms due to inclusion of zero-point energy is a broadening. For the present system where a large fraction of the molecules experience multiple collisions

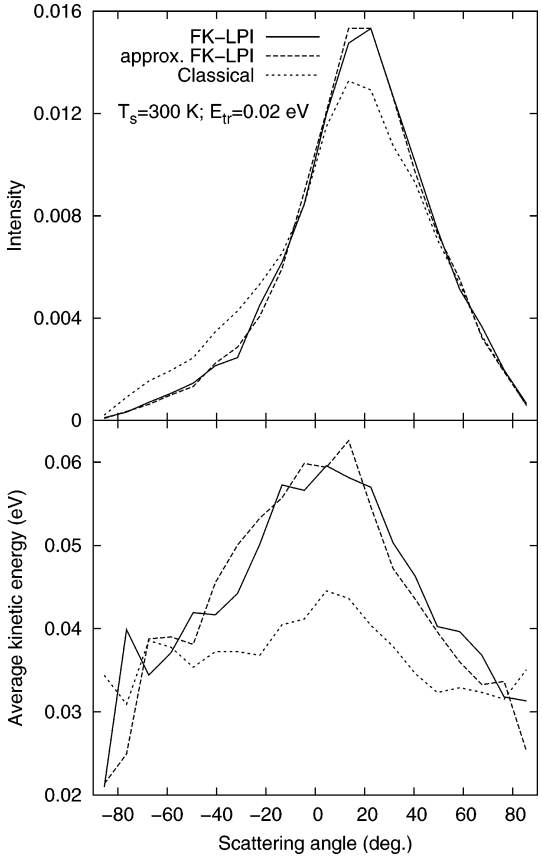

Figure 5. Angular distributions for H_2O scattering from graphite and average final kinetic energy as a function of the scattering angle. Initial conditions: $T_s = 300$ K, $E_{tr} = 0.02$ eV. Solid lines, accurate FK-LPI; dashed lines, approximate FK-LPI; dotted lines, classical.

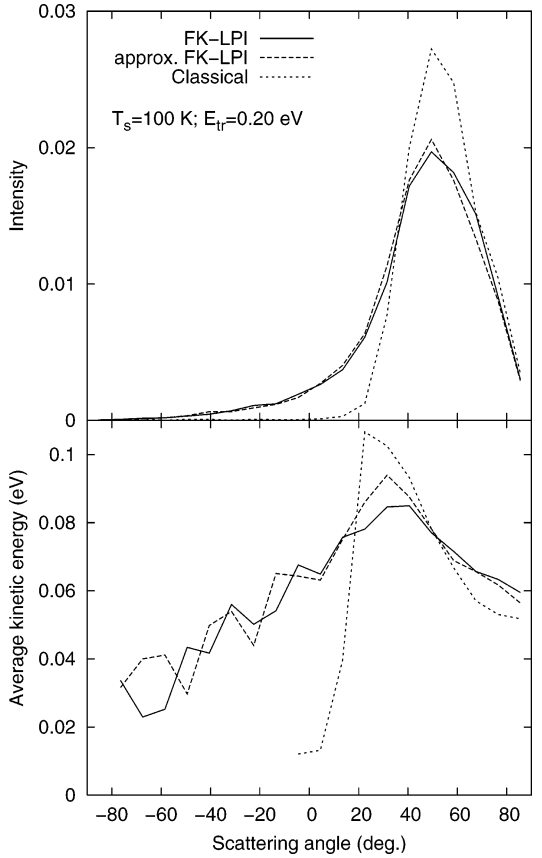

Figure 6. Angular distributions for H_2O scattering from graphite and average final kinetic energy as a function of the scattering angle. Initial conditions: $T_s = 100$ K, $E_{tr} = 0.20$ eV. Solid lines, accurate FK-LPI; dashed lines, approximate FK-LPI; dotted lines, classical.

with the surface a difference in residence time also becomes an important factor, which explains why the FK-LPI distributions in Figures 4 and 5 are more narrow than the classical distributions. The residence time is much longer in the classical case, leading to a more complete thermalization.[38] At 100 K, however, most of the trapped molecules stick to the surface in the classical case leading to a narrow distribution corresponding essentially to direct scattering. From Figure 8 it is clear that classical or quantum mechanical sampling of the surface initial conditions does not affect the probability of direct scattering but has a large effect on the time the transiently trapped molecules spend on the surface.

We have previously observed that the number of molecules remaining on the surface as a function of time follows first-order kinetics.[37,39] The molecules are only partially equilibrated to the surface temperature,[38] but the equilibration for the translational motion in the surface normal direction is fast, leading to a desorption-like process. This behavior is observed in Figure 9a for a surface temperature of 300 K and a collision energy of 0.02 eV when classical sampling is used. Molecules with a surface residence time longer than 2.5 ps (and more than three collisions with the surface) have been included in the analysis. A desorption rate coefficient equal to 3.6×10^{10} s^{-1} is obtained from a linear fit to the data. This value differs somewhat from the result presented in ref 39. The main reason is the much better statistics in the present case (7814 trajectories compared to 794), but the different crystal size and initial conditions probably also contribute.

The difference between the classical and the FK-LPI results is striking. In Figure 9a, we observe that the FK-LPI trapping probability is a nonexponential function of time, i.e., not following simple rate kinetics. Why? Since the LPI model employs classical dynamics, we expect the FK-LPI desorption rate at some time t to (just as in a normal classical simulation) increase with growing instantaneous kinetic energy in the normal direction. However, from Figure 3b we have already seen that this kinetic energy increases (a similar behavior is seen for $T_s = 300$ K).

The extraction of a rate constant from the FK-LPI results may be done in two ways. First we consider a polynomial fit procedure. Since FK-LPI is accurate for short times, one may fit the early FK-LPI curve in Figure 9a to a polynomial in t and extract the linear slope when $t \rightarrow 0$. The curve should be linear at early times if the rate obeys simple kinetics. By fitting the data between 2.5 and 10 ps in Figure 9a to a polynomial of second degree, a rate coefficient equal to 6.4×10^{10} s^{-1} is obtained when extrapolating to $t = 0$. Hence, the slope at short times reflects the (correct) desorption rate coefficient before the Wigner distribution has degraded significantly.

Next, we try extracting the rate coefficient from a rate equation analysis. The z-component of the kinetic energy is in classical terms proportional to the z-component of the temperature. From a graph similar to Figure 3b, but representing the $T = 300$ K case, the time-dependence of the kinetic energy in the normal direction can rather accurately be described using the equation

$$T(t) = T_\infty(1 - be^{-ct}) \tag{23}$$

with $T_\infty = 710$ K, $b = 0.3183$ and $c = 0.1349$ ps^{-1}. If the instantaneous desorption rate, $k(t)$, follows a phenomenological type of Arrhenius equation, then $k(t)$ should depend on the

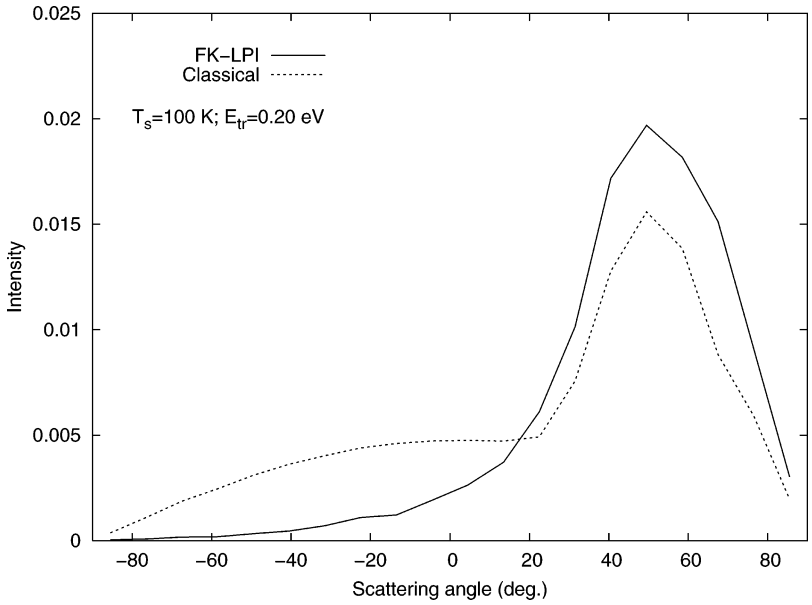

Figure 7. Angular distribution for H_2O scattering from graphite. Initial conditions: $T_s = 100$ K, $E_{tr} = 0.20$ eV. Solid line, accurate FK-LPI (from Figure 6); dotted line, classical. The classical distribution is a superposition of the inelastic distribution from Figure 6 and a thermal desorption cosine distribution.

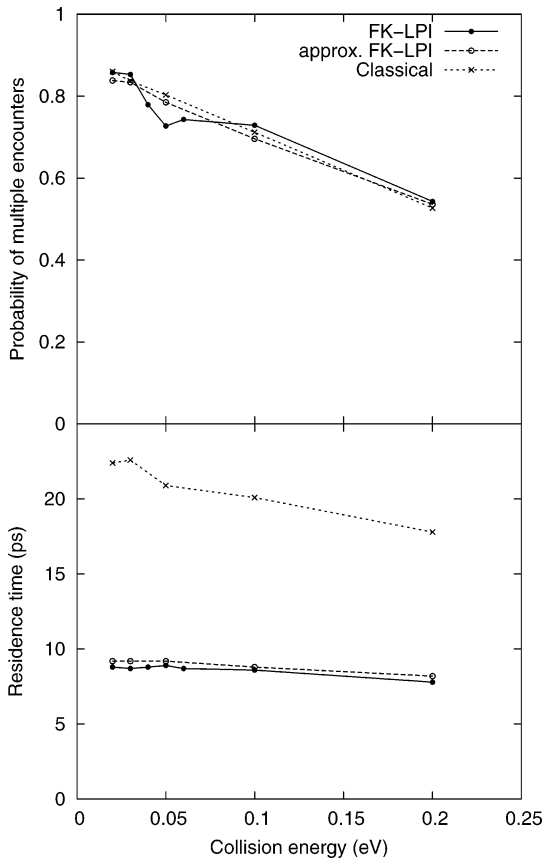

Figure 8. The probability of multiple H_2O−surface encounters and average residence time for transiently trapped molecules as a function of collision energy. Surface temperature: 300 K. Solid lines, accurate FK-LPI; dashed lines, approximate FK-LPI; dotted lines, classical.

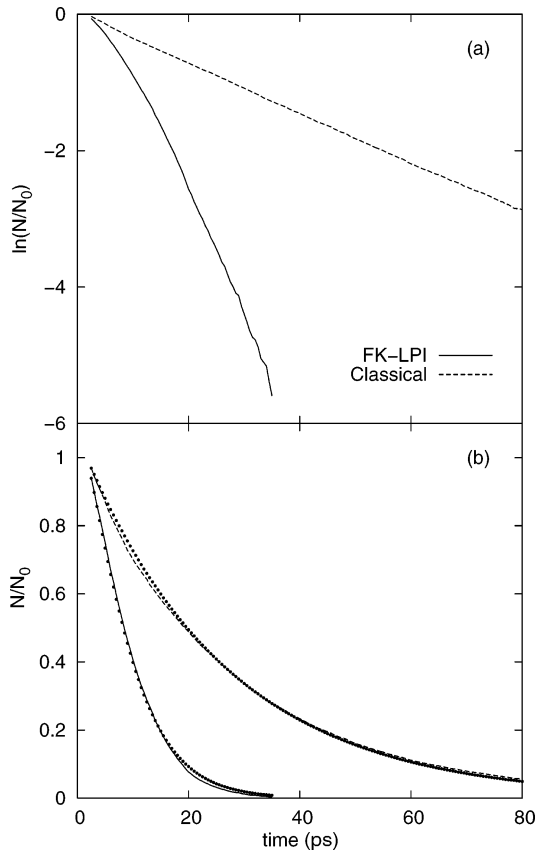

Figure 9. (a) The logarithm of the fraction of molecules trapped on the surface as a function of time for $T_s = 300$ K, $E_{tr} = 0.02$ eV. (b) The same data plotted on a linear scale together with results from the simple desorption model described in the text (dotted curves).

kinetic energy in the normal direction in the following classical manner:

$$k(t) = k(0)\exp\left[-\frac{D}{k_B}\left(\frac{1}{T(t)} - \frac{1}{T(0)}\right)\right] \qquad (24)$$

where $D = 0.125$ eV is the binding energy (section 3.1), and $T(t)$ is the instantaneous kinetic energy rephrased in terms of temperature. The desorption kinetics may now be simulated using the equation

$$-\frac{dN}{dt} = k(t)N \qquad (25)$$

TABLE 1: Desorption-like Rate Coefficients for Scattering at 0.02 eV from Graphite at 100 and 300 K[a]

	$k(T)/10^{10}$ s^{-1}	
T_s/K	classical	FK-LPI
100		1.7
300	3.8	6.2

[a] The rate coefficients are estimated using the rate equation approach described in the text.

which can easily be integrated from given initial conditions (N/N_0 at $t_0 = 2.5$ ps) provided $k(0)$ is known. The results shown as dotted curves in Figure 9b have been obtained by finding the $k(0)$-values that minimize the difference between the original data and the solution to eq 25. In the classical case (for which k is time-independent) we obtain $k = 3.8 \times 10^{10}$ s^{-1}. The small difference compared with the linear fit reflects the sensitivity to the initial condition. In the FK-LPI case the best fit is obtained for $k(0) = 6.2 \times 10^{10}$ s^{-1}. This rate equation analysis yields an estimate which agrees quite well with the polynomial fit procedure. It shows that the nonlinear Arrhenius plot can be explained with the increase in surface kinetic energy in the normal direction.

For a surface temperature of 100 K and using classical sampling almost all trapped molecules stick to the surface and a desorption rate coefficient cannot be determined. This is expected since the half-life in this case is increased from less than 20 ps to approximately 0.3 μs. The rate coefficient in the FK-LPI case obtained as described above is approximately a factor of 3 smaller at 100 K compared to 300 K, see Table 1.The redistribution of zero-point energy from in-plane to out-of-plane motion will also affect the angular distributions, in particular for low collision energies where the available energy is small and the trapping probability large. We expect the effect on the intensity to be rather small: more surface kinetic energy broadens the distribution but simultaneously reduces the residence time which narrows the distribution. The average final kinetic energy will increase due to the energy redistribution, and the increasing energy in the surface normal direction may also manifest itself as zero-point energy leakage from the surface to the molecule.

The effect on the distributions in Figures 4 and 6 is expected to be small due to the rather high collision energy (0.20 eV). Energy transfer is from molecular translation and rotation to the surface degrees of freedom in these cases. The average de-excitation is about 100 meV using classical sampling and 10−20 meV lower in the quantum case. At 300 K and 0.02 eV, Figure 5, the water molecule (rotation plus translation) is excited by 27 meV when classical sampling is used and by 53 meV in the FK-LPI case. At this temperature the thermal energy is 183 meV per surface atom (13 meV larger than the zero-point energy), i.e., the observed excitation is not unreasonable. If only trajectories with one collision with the surface are considered, the FK-LPI result is reduced by 50% to 26 meV while the classical result is reduced by only 30% to 20 meV. It turns out that the average excitation increases approximately linearly with the number of surface collisions up to $N \sim 10$ but the increase is about five times faster in the FK-LPI case. Increased kinetic energy in the normal direction due to energy redistribution within the graphite crystal is likely part of the explanation for the difference observed between classical and FK-LPI sampled trajectories. It should be noted, however, that the erroneous kinetic energy increase is much smaller at 300 K (47%) compared to the 100 K case shown in Figure 3b (81%).

The most critical case regarding zero-point energy leakage is the result at 100 K and 0.02 eV. Results using these initial conditions are presented in Table 1 in the form of desorption rate coefficients corrected for energy redistribution within the crystal. Under these conditions the energy transfer must be from the molecule to the surface since essentially no thermal surface energy is available. As mentioned above we cannot obtain classical results in this case due to almost complete sticking. Using the approximate FK-LPI method the average excitation after one collision was indeed found to be very close to zero (2 meV), i.e., the zero point energy (ca. 170 meV per surface atom) is essentially conserved. Most trajectories are transiently trapped under these conditions (92%) and the trapped trajectories stay on the surface for 16 ps on average, resulting in a broad angular distribution. The average energy transfer for all trajectories was 47 meV.

In order to obtain a crude estimate of the effect of energy redistribution, we repeated the calculation with artificial scaling

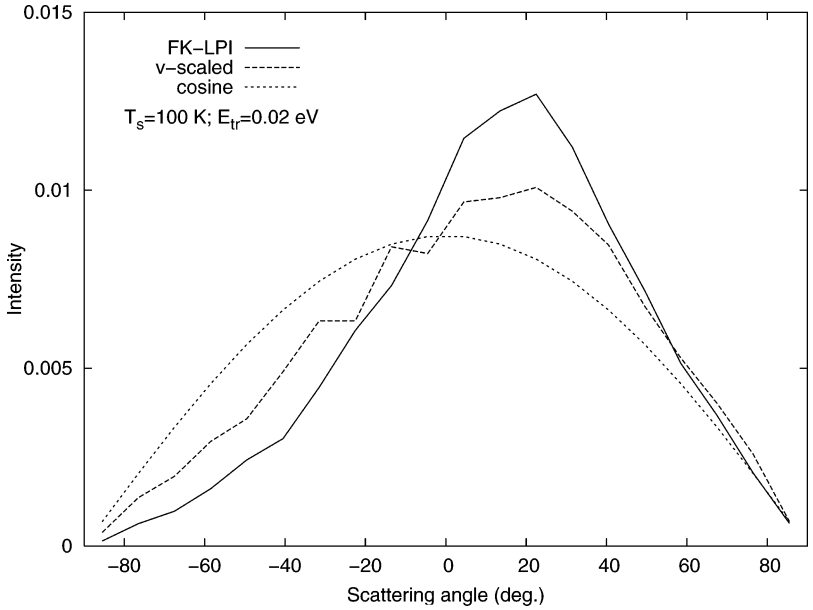

Figure 10. Angular distribution for H_2O scattering from graphite. Initial conditions: $T_s = 100$ K, $E_{tr} = 0.02$ eV. Solid line, FK-LPI; dashed line, velocity-scaled FK-LPI (see text); dotted line, a cosine distribution.

of the surface atom velocities after each integration step in order to conserve the kinetic energies in the *x* -, *y*- and *z*-directions. The angular distribution does not change qualitatively but becomes broader, Figure 10. The peak is still at roughly 20° and both the "scaled'' and the FK-LPI distribution clearly deviate from the cosine form expected in the purely classical case if thermal desorption is assumed.

The final average speed decreases, in particular for scattering in the normal direction. The total energy transfer from the surface to molecular translation plus rotation decreases from 47 to 27 meV despite the fact that the residence time on the surface for trapped trajectories increases to 39 ps. Only a small fraction of the collisions are direct (5%) but these are essentially elastic (average molecular de-excitation: 0.3 meV).

No quantitative conclusions can be drawn from the crude "velocity-scaled'' calculations described above, but the results indicate that a large part of the zero-point energy leakage observed for the lowest temperature and collision energy is caused by the energy redistribution within the graphite crystal. This increases the final average speed but has a rather small effect on the angular intensity distribution.

5. Conclusions

We have applied the linearized path integral (LPI) approximation in order to include quantum effects into the simulation of the scattering and trapping process of a water molecule colliding with a graphite surface. The system was studied for rather low collision energies (0.02−0.20 eV) where the probability of trapping, defined as multiple collisions with the surface, is high. The trapping probability was not affected by quantizing the surface initial conditions.

The surface was studied at temperatures of 100 and 300 K. At 300 K and 0.02 eV collision energy the FK-LPI angular distribution was found to be more narrow than the corresponding classical distribution. The reason is that the transiently trapped molecules remain on the surface for a considerably shorter time in the quantum case. The equilibration to the surface temperature is less complete, leading to a more peaked angular distribution. At 100 K a large difference between results corresponding to quantum and classical initial conditions was observed also for the higher collision energy of 0.20 eV. The classical distribution is now more narrow since almost all molecules experiencing multiple collisions stick to the surface in the classical case. The classical distribution is therefore dominated by direct scattering while the quantum distribution still has a large contribution from transiently trapped molecules. We cannot compare directly with the experimental results from ref 39 since either the surface temperature or the collision energy was too high for quantum effects to significantly affect the angular distributions. Such a detailed comparison would also require a more accurate potential than we have used in the present study.

It was shown that the LPI results, when corrected for the redistribution of kinetic energy between parallel and perpendicular motion of the surface atoms, are consistent with a simple kinetic model, predicting a desorption rate constant at 300 K being more than 60% larger than the classical prediction. At 100 K, the LPI desorption rate constant has decreased by a factor of 3 while a classical simulation is unable to produce a rate constant due to indefinite sticking of the water molecules.

Finally, results from a crude velocity rescaling implementation of the FK-LPI method, which conserves the initial surface atom kinetic energy partitioning, suggests that the angular intensity distributions are not severely affected by the kinetic energy redistribution even in cases where the effect on the average final speed is significant.

The largest problem with the LPI approximation was in the present application the drift in kinetic energy in the direction normal to the surface. This is due to the well-known fact that the LPI dynamics does not "conserve the ensemble''. The drift is in the case of graphite particularly pronounced since the force constants of the graphite surface *in the plane* are much larger than the constants characterizing the *out of plane* movements. Hence, more zero point motion is added in plane and, when doing the approximate classical dynamics, energy will then flow from in plane to out of plane movements. In surfaces where the force constants in plane and out of plane are similar, e.g., metals or diamond, this drift problem will be expected to be very small.

We end by noting that the gradient implementation of the Feynman-Kleinert Wigner transform[47] depends on the particular system at hand only through a standard MD force routine. Hence one may easily simulate other surfaces by just replacing the "black-box'' force routine by another.

Acknowledgment. This research is supported by the Swedish Research Council (VR).

References and Notes

(1) Gross, A.; Wilke, S.; Scheffler, M. *Phys. Rev. Lett*. **1995**, *75*, 2718.
(2) Kroes, G. J.; Baerends, E. J.; Mowrey, R. C. *Phys. Rev. Lett*. **1997**, *78*, 3583.
(3) Kroes, G. J.; Baerends, E. J.; Mowrey, R. C. *J. Chem. Phys*. **1997**, *107*, 3309.
(4) Dai, J.; Light, J. C. *J. Chem. Phys*. **1997**, *107*, 1676.
(5) Gross, A.; Scheffler, M. *Phys. Rev. B* **2000**, *61*, 8425.
(6) Pijper, E.; Somers, M. F.; Kroes, G. J.; Olsen, R. A.; Baerends, E. J.; Busnengo, H. F.; Salin, A.; Lemoine, D. *Chem. Phys. Lett*. **2001**, *347*, 277.
(7) Mowrey, R. C.; McCormack, D. A.; Kroes, G. J.; Baerends, E. J. *J. Chem. Phys*. **2001**, *114*, 7581.
(8) Somers, M. F.; McCormack, D. A.; Kroes, G. J.; Olsen, R. A.; Baerends, E. J.; Mowrey, R. C. *J. Chem. Phys*. **2002**, *117*, 6673.
(9) Vincent, J. K.; Olsen, R. A.; Kroes, G. J.; Baerends, E. J. *Surf. Sci.* **2004**, *573*, 433.
(10) van Harrevelt, R.; Manthe, U. *J. Chem. Phys.* **2005**, *123*, 124706.
(11) Rivière, P.; Somers, M. F.; Kroes, G. J.; Martín, F. *Phys. Rev. B* **2006**, *73*, 205417.
(12) Watts, E.; Sitz, G. O. *J. Chem. Phys*. **2001**, *114*, 4171.
(13) Wang, Z. S.; Darling, G. R.; Holloway S. *J. Chem. Phys.* **2004**, *120*, 2923.
(14) Billing, G. D. *Dynamics of Molecule Surface Interactions*; Wiley: New York, 2000.
(15) Pesce, L.; Saalfrank, P. *Chem. Phys*. **1997**, *219*, 43.
(16) Cerjan, C.; Kosloff, R. *Phys. Rev. B* **1986**, *34*, 3832.
(17) Saalfrank, P.; Kosloff, R. *J. Chem. Phys*. **1996**, *105*, 2441.
(18) Pesce, L.; Saalfrank, P. *J. Chem. Phys.* **1998**, *108*, 3045.
(19) Nest, M.; Saalfrank, P. *J. Chem. Phys*. **2000**, *113*, 8753.
(20) Beyvers, S.; Ohtsuki, Y.; Saalfrank, P. *J. Chem. Phys.* **2006**, *124*, 234706.
(21) Pollard, W. T.; Friesner, R. A. *J. Chem. Phys*. **1994**, *100*, 5054.
(22) Jackson, B. *Chem. Phys. Lett*. **1997**, *270*, 484.
(23) Jackson, B. *J. Chem. Phys*. **1998**, *108*, 1131.
(24) Medina, Z.; Jackson, B. *J. Chem. Phys*. **2006**, *125*, 224703.
(25) Nest, M.; Meyer, H.-D. *J. Chem. Phys*. **2003**, *119*, 24.
(26) Jackson, B. *Chem. Phys. Lett*. **1999**, *308*, 456.
(27) Wang, Z. S.; Darling, G. R.; Jackson, B.; Holloway, S. *J. Phys. Chem. B* **2002**, *106*, 8422.
(28) Jackson, B. *J. Chem. Phys.* **1989**, *90*, 140.
(29) Bittner, E. R.; Light, J. C. *J. Chem. Phys*. **1993**, *99*, 8229.
(30) Tully, J. C. *J. Chem. Phys.* **1980**, *73*, 1975.
(31) Dohle, M.; Saalfrank, P.; Uzer, T. J. *Chem. Phys.* **1998**, *108*, 4226.
(32) Park, S. C.; Bowman, J. M. *Chem. Phys. Lett*. **1985**, *119*, 275.
(33) Jackson, B. *J. Chem. Phys.* **1990**, *92*, 1458.
(34) Adhikari, S.; Billing, G. D. *J. Chem. Phys*. **2000**, *112*, 3884.
(35) Sha, X.; Jackson, B.; Lemoine, D.; Lepetit, B. *J. Chem. Phys*. **2005**, *122*, 014709.
(36) Kerwin, J.; Sha, X.; Jackson, B. *J. Phys. Chem. B* **2006**, *110*, 18811.
(37) Någård, M. B.; Andersson, P. U.; Marković, N.; Pettersson, J. B. C. *J. Chem. Phys*. **1998**, *109*, 10339.

(38) Någård, M. B.; Marković, N.; Pettersson, J. B. C. *J. Chem. Phys.* **1998**, *109*, 10350.
(39) Marković, N.; Andersson, P. U.; Någård, M. B.; Pettersson, J. B. C. *Chem. Phys.* **1999**, *247*, 413; **2000**, *252*, 409 (erratum).
(40) Tomsic, A.; Marković, N.; Pettersson, J. B. C. *Phys. Chem. Chem. Phys.* **2001**, *3*, 3667.
(41) Tomsic, A.; Andersson, P. U.; Marković, N.; Piskorz, W.; Svanberg, M.; Pettersson, J. B. C. *J. Chem. Phys.* **2001**, *115*, 10509.
(42) Tomsic, A.; Marković, N.; Pettersson, J. B. C. *J. Phys. Chem. B* **2003**, *107*, 10576.
(43) Poulsen, J. A.; Nyman, G.; Rossky, P. J. *J. Chem. Phys.* **2003**, *119*, 12179.
(44) Poulsen, J. A.; Nyman, G.; Rossky, P. J. *J. Phys. Chem. B* **2004**, *108*, 19799.
(45) Poulsen, J. A.; Nyman, G.; Rossky, P. J. *J. Phys. Chem. A* **2004**, *108*, 8743.
(46) Poulsen, J. A.; Nyman, G.; Rossky, P. J. *Proc. Natl. Acad. Sci. U.S.A.* **2005**, *102*, 6709.
(47) Poulsen, J. A.; Nyman, G.; Rossky, P. J. *J. Chem. Theory Comput.* **2006**, *2*, 1482.
(48) Poulsen, J. A.; Scheers, J.; Nyman, G.; Rossky, J. P. *Phys. Rev. B* **2007**, *224505*.
(49) Wigner, E. *Phys. Rev.* **1932**, *40*, 749.
(50) Sun, X.; Wang, H.; Miller, W. H. *J. Chem. Phys.* **1998**, *109*, 4190.
(51) Heller, E. J. *J. Chem. Phys.* **1976**, 65, 1289.
(52) Hernandez, R.; Voth, G. A. *Chem. Phys.* **1998**, *233*, 243.
(53) Sun, X.; Miller, W. H. *J. Chem. Phys.* **1997**, *106*, 916.
(54) Feynman, R. P.; Kleinert, H. *Phys. Rev. A* **1986**, *34*, 5080.
(55) Jang, S.; Voth, G. A. *J. Chem. Phys.* **1999**, *111*, 2357.
(56) Brenner, D. W. *Phys. Rev. B* **1990**, *42*, 9458; *Phys. Rev. B* **1992**, *46*, 1948 (erratum).
(57) Coker, D. F.; Watts, R. O. *J. Phys. Chem.* **1987**, *91*, 2513.
(58) Allen, M. P.; Tildesley, D. J. In *Computer Simulations of liquids*; Oxford University Press: Oxford, U.K., 1987.
(59) Andersson, P. U.; Någård, M. B.; Bolton, K.; Svanberg, M.; Pettersson, J. B. C. *J. Phys. Chem. A* **2000**, *104*, 2681.